

1            **Intermediate-magnitude postseismic slip follows**  
2            **intermediate-magnitude ( $M$  4 to 5) earthquakes in**  
3            **California**

4            **M. A. Alwahedi<sup>1,2</sup>, J. C. Hawthorne<sup>3</sup>**

5            <sup>1</sup>School of Earth and Environment, University of Leeds, Leeds, UK

6            <sup>2</sup>Now at Institute for Risk and Disaster Reduction, University College London, London, UK

7            <sup>3</sup>Department of Earth Sciences, University of Oxford, Oxford, UK

8            **Key Points:**

- 9            • We examine postseismic slip following M4-5 earthquakes using borehole strain data  
10           • The median estimated postseismic moment is 0.4 times the coseismic moment  
11           • The postseismic moment ratio is intermediate between estimates for small and large  
12           earthquakes

---

Corresponding author: J. C. Hawthorne, [jessica.hawthorne@earth.ox.ac.uk](mailto:jessica.hawthorne@earth.ox.ac.uk)

13 **Abstract**

14 The magnitude of postseismic slip is useful for constraining physical models of fault  
 15 slip. Here we examine the postseismic slip following intermediate-magnitude ( $M$  4 to 5)  
 16 earthquakes by systematically analyzing data from borehole strainmeters in central and  
 17 northern California. We assess the noise in the data and identify 36 records from 12 earth-  
 18 quakes that can be interpreted. We estimate postseismic to coseismic moment ratios by  
 19 comparing the coseismic strain changes with strain changes induced by afterslip in the  
 20 following 1.5 days. The median estimated postseismic moment is 0.36 times the coseis-  
 21 mic moment, with a 90% confidence interval between 0.22 and 0.54. This postseismic  
 22 moment is slightly larger than typically observed following large ( $M > 6$ ) earthquakes  
 23 but smaller than observed following small ( $M$  2 to 4) earthquakes. The intermediate-  
 24 magnitude postseismic slip suggests a size dependence in the dynamics of earthquakes  
 25 or in the properties of fault areas that surround earthquakes.

26 **1 Introduction**

27 Deformation in the hours to years following earthquakes accumulates via a range  
 28 of processes, including afterslip, poroelastic flow, and viscoelastic deformation. After-  
 29 slip is usually the largest cause of deformation in the first few hours to months. The af-  
 30 terslip that accumulates following large ( $M > 6$ ) earthquakes typically has moment equal  
 31 to 10 to 30% of the coseismic moment (e.g., Cetin et al., 2012; D’Agostino, Cheloni, Fornaro,  
 32 Giuliani, & Reale, 2012; Donnellan & Lyzenga, 1998; Gahalaut et al., 2008; Gonzalez-  
 33 Ortega et al., 2014; Johanson & Bürgmann, 2010; Lin et al., 2013; Segall, Bürgmann,  
 34 & Matthews, 2000), though afterslip moments for individual earthquakes range from a  
 35 few percent to several hundred percent of the coseismic moment (see Figure 4, Bürgmann  
 36 et al. (2001); Dogan et al. (2014); Freed (2007); Langbein, Murray, and Snyder (2006);  
 37 Paul, Lowry, Bilham, Sen, and Smalley (2007)).

38 While afterslip moments vary, the postseismic to coseismic moment ratios estimated  
 39 for large earthquakes show no systematic trend with magnitude (see Lin et al. (2013),  
 40 Fattahi, Amelung, Chaussard, and Wdowinski (2015), and Figure 4 for summaries). The  
 41 inferred magnitude-independent afterslip is consistent with a self-similar model of earth-  
 42 quakes, where large events are scaled versions of smaller ones. However, large afterslip  
 43 following small earthquakes has been proposed to explain the long recurrence intervals  
 44 of small repeating earthquakes (Chen & Lapusta, 2009), and analysis of small ( $M$  1.9  
 45 to 3.5) earthquakes near San Juan Bautista, CA revealed that those small earthquakes  
 46 had afterslip with moment roughly equal to the coseismic moment, on average (Hawthorne,  
 47 Simons, & Ampuero, 2016). Those large afterslip moments could simply indicate that  
 48 the frictional properties of the San Andreas Fault near San Juan Bautista region are un-  
 49 usual, and more prone to large afterslip. Afterslip with moment 1.5 to 3 times the co-  
 50 seismic moment was identified following several larger earthquakes in the area: the 2004  
 51  $M$  6 Parkfield earthquake (Barbot, Fialko, & Bock, 2009; Freed, 2007; Langbein et al.,  
 52 2006), the 2007  $M$  5.4 Alum Rock earthquake (Murray-Moraleda & Simpson, 2009), and  
 53 the 1998  $M$  5.1 San Juan Bautista earthquake (Taira, Bürgmann, Nadeau, & Dreger,  
 54 2014).

55 But the large afterslip moments identified following  $M < 3.5$  earthquakes could  
 56 also indicate that small earthquakes generally behave differently—that the self-similar  
 57 scaling of postseismic slip breaks down as earthquakes become smaller. For example, the  
 58 afterslip moment could change as earthquake rupture extents become smaller than the  
 59 seismogenic zone width, so that most afterslip occurs within the seismogenic zone, rather  
 60 than above and below it. Or the afterslip moment could change as earthquake rupture  
 61 extents become similar to the minimum earthquake nucleation size, and thus become too  
 62 small to drive more rapid slip (Chen & Lapusta, 2009).

In this study, we further examine how afterslip moment varies with earthquake size by examining intermediate-magnitude ( $M$  4 to 5) earthquakes. Only a few afterslip moments have been estimated for  $M$  4 to 6 earthquakes, and all reported values are large. Afterslip moments between 1 and 5 times the coseismic moment were observed following  $M$  4.7 to 5.5 earthquakes on the Chaman fault (Furuya & Satyabala, 2008), on the Ghazaband fault (Fattahi et al., 2015), near Alum Rock, CA (Murray-Moraleda & Simpson, 2009), and near Mogul, NV (Bell, Amelung, & Henry, 2012). However, these large afterslip moments could reflect a reporting bias, as smaller amounts of afterslip would be difficult to observe.

Here we use high-precision borehole strain data to examine postseismic slip following  $M$  4 to 5 earthquakes in central and northern California. We systematically identify earthquakes with resolvable coseismic deformation at each of 12 strainmeters in the PBO and USGS networks. We are able to assess the afterslip moment with reasonable accuracy for 12 earthquakes. The median afterslip moment is roughly 0.4 times the coseismic moment, between the values obtained for smaller and larger earthquakes.

## 2 Available Data and Earthquakes

We examine data from 12 strainmeters located along the San Andreas Fault in California, shown in Figure 1. More than half of the high-quality earthquake records will come from strainmeter SJT, which was installed by the USGS in 1983 at the northern end of the central creeping section of the San Andreas Fault Gladwin, Gwyther, Hart, Francis, and Johnston (1987). The remaining records come from strainmeters that were installed by UNAVCO as part of the Plate Boundary Observatory (PBO). We consider data from 11 PBO strainmeters installed between 2006 and 2008. Strainmeters B073, B075, B076, B078, and B079 are located near Parkfield, at the southern edge of the central creeping section, while strainmeters B058, B065, and B067 are located near San Juan Bautista, at the northern edge of the central creeping section, and strainmeters B045, B934, and B935 are located close to the Mendocino triple junction, near another creeping section of the San Andreas.

Small earthquakes occur frequently along these creeping sections, mostly at depths of 4 to 15 km (e.g., Irwin & Barnes, 1975; Waldhauser & Schaff, 2008). We begin our analysis by identifying all  $M$  4 to 6 earthquakes that occurred within 30 km of the strainmeters while the strainmeters were operating, as recorded in the NCSN catalog. This identification recovers 112 potential earthquake-station pairs, or 112 potential earthquake records. But we will find that only 14 records, which cover 12 unique earthquakes, have low enough noise level that we can usefully assess the magnitude of afterslip.

## 3 Initial Data Processing

The deformation produced by co- and postseismic slip are recorded at the strainmeters via three to four horizontal extensometers, which are located at depths of 150 to 250 m and measure changes in the horizontal borehole width at various azimuths. SJT records deformation at 18-minute intervals, and we use 10-minute data from the PBO strainmeters. We convert the time-varying extensometer measurements to the three time-varying horizontal components of strain  $\varepsilon_{E+N}$ ,  $\varepsilon_{E-N}$ , and  $\varepsilon_{2EN}$  using the tidal calibrations derived by J. Langbein for strainmeter SJT and by Hodgkinson, Langbein, Henderson, Mencin, and Borsa (2013) for the PBO strainmeters.

We will directly analyze the time series of  $\varepsilon_{E+N}$ ,  $\varepsilon_{E-N}$ , and  $\varepsilon_{2EN}$  recorded at strainmeter SJT. But for the PBO strainmeters, we analyze different linear combinations of these strain components. All the strain components are recorded with high instrumental precision, less than 1 nanostrain. But the various components of strain have different sensitivity to atmospheric and hydrologic noise. So we follow the approach of Hawthorne,

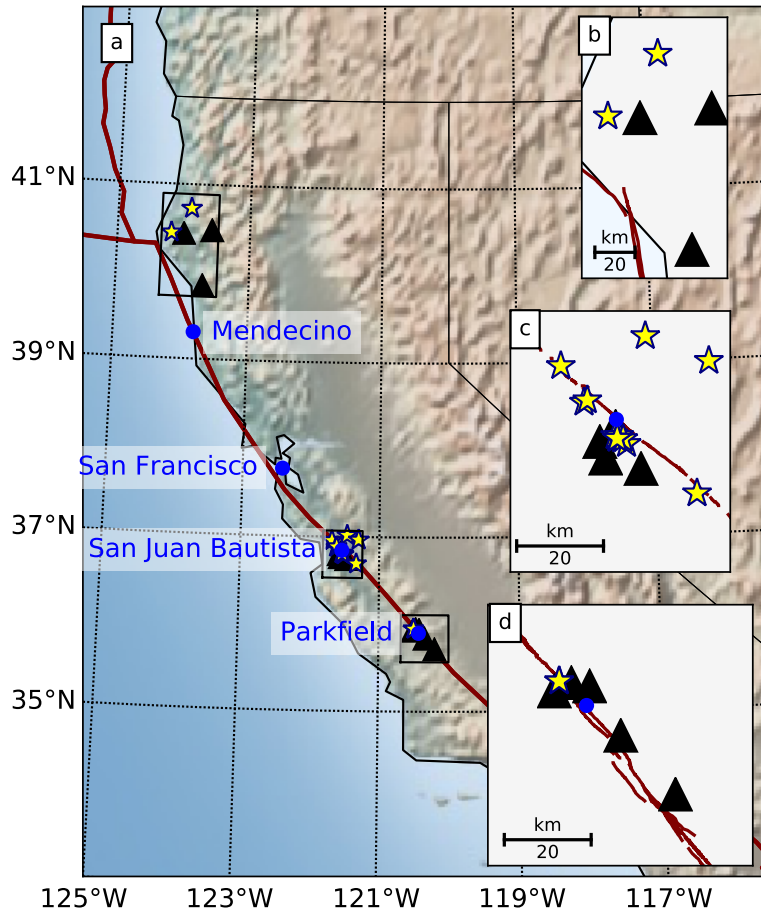


**Figure 1.** (a) Map of the central San Andreas Fault system in California. In all plots, black triangles are strainmeter locations, yellow stars are the earthquakes for which we estimate post-seismic signals, blue circles are cities, and the red lines mark the plate boundary. (b), (c), and (d) Maps of the three clusters of strainmeters. The strainmeters in each panel are, from west to east, (b) B045, B934, and B935; (c) B058, B067, SJT, and B065; (d) B075, B073, B076, B078, and B079. Note that the marker for SJT is behind the central group of earthquakes in panel c.

112 Bostock, Royer, and Thomas (2016) to identify linear combinations of  $\varepsilon_{E+N}$ ,  $\varepsilon_{E-N}$ , and  
 113  $\varepsilon_{2EN}$  that are normally less noisy: the components that have minimal response to at-  
 114 mospheric pressure variations. We refer to the linear combinations that are closest to  
 115 the original components as  $\varepsilon_{E+N-na}$ ,  $\varepsilon_{E-N-na}$ , and  $\varepsilon_{2EN-na}$ , and we will analyze all  
 116 three time series at the PBO strainmeters, though we note that only two of these three  
 117 components are independent. The third component is a linear combination of the first  
 118 two.

119 Having isolated the strain components of interest, we estimate and remove several  
 120 non-tectonic signals from each time series, following, for example, Hart, Gladwin, Gwyther,  
 121 Agnew, and Wyatt (1996); Langbein (2010); Roeloffs (2010), and Hawthorne, Bostock,  
 122 et al. (2016). To remove borehole curing signals, we discard the first 18 months of data  
 123 at each station and then fit and remove a linear trend and a decaying exponential with  
 124 time constant around 1 year. Then we estimate and remove shorter-timescale nontec-  
 125 tonic variations. We compare the tidal model of Cartwright and Edden (1973) with the  
 126 data and identify tidal frequencies that are likely to have tidal signals with amplitudes  
 127 of at least 0.5 times the noise level. We estimate best-fitting sinusoids at those frequen-  
 128 cies and remove them. At SJT, we also estimate and remove a linear response to atmo-  
 129 spheric pressure and a periodic 3-hour signal that is likely instrumental noise, as iden-  
 130 tified by Hawthorne, Simons, and Ampuero (2016).

#### 131 4 Interpreting Example Strain Records

132 After removing these non-tectonic signals, we can analyze the earthquake- and afterslip-  
 133 induced strain. Several examples of the co- and postseismic strain are shown in Figures 2  
 134 and S1-S18. Figure 2a shows a high quality record of a  $M$  4.2 earthquake located about  
 135 5 km NE of strainmeter B067. An abrupt coseismic strain step is followed by the grad-  
 136 ual accumulation of postseismic strain over the two days shown. Figure 2b shows a sim-  
 137 ilar record of a  $M$  4.0 earthquake located about 5 km SE of strainmeter SJT, but here  
 138 the signal to noise ratio is lower.

139 In our modelling, we will assume that the postseismic strain is created by after-  
 140 slip. If afterslip occurs in an area within 1 to 2 earthquake radii of the earthquake rup-  
 141 ture, as is usually observed following large earthquakes (D'Agostino et al., 2012; Ryder,  
 142 Parsons, Wright, & Funning, 2007), and if the earthquake radius is small relative to the  
 143 earthquake-strainmeter distance, then the co- and postseismic slip should appear co-located  
 144 from the perspective of the strain observations. In other words, the co- and postseismic  
 145 slip should have approximately the same Green's functions. Such similar Green's func-  
 146 tions are consistent with the data in Figure 2. The ratio of postseismic to coseismic strain  
 147 is similar on the three strain components, as expected if the strains are given by mul-  
 148 tiplying the co- and postseismic moments by the same Green's functions.

149 In this study, we are interested in the ratio of the postseismic moment to the co-  
 150 seismic moment. If the Green's functions are the same, the moment ratio can be obtained  
 151 simply by dividing the postseismic strain by the coseismic strain. In Figure 2a, for in-  
 152 stance, we may note that the postseismic strains accumulated within 2 days of the earth-  
 153 quake have magnitude about 20% of the amplitude of the coseismic strains. Such strain  
 154 ratios suggest that the afterslip moment accumulated within 2 days of the earthquake  
 155 is equal to about 20% of the coseismic moment.

#### 156 5 Identifying Interpretable Strain Records

157 Our search for earthquakes within 30 km of the strainmeters revealed 112 poten-  
 158 tial earthquake records. But most of these are not interpretable. First, many are too noisy.  
 159 In our initial culling of the data, we visually examine the 112 earthquake records and  
 160 retain only those where the coseismic offset is well resolved on at least one component.

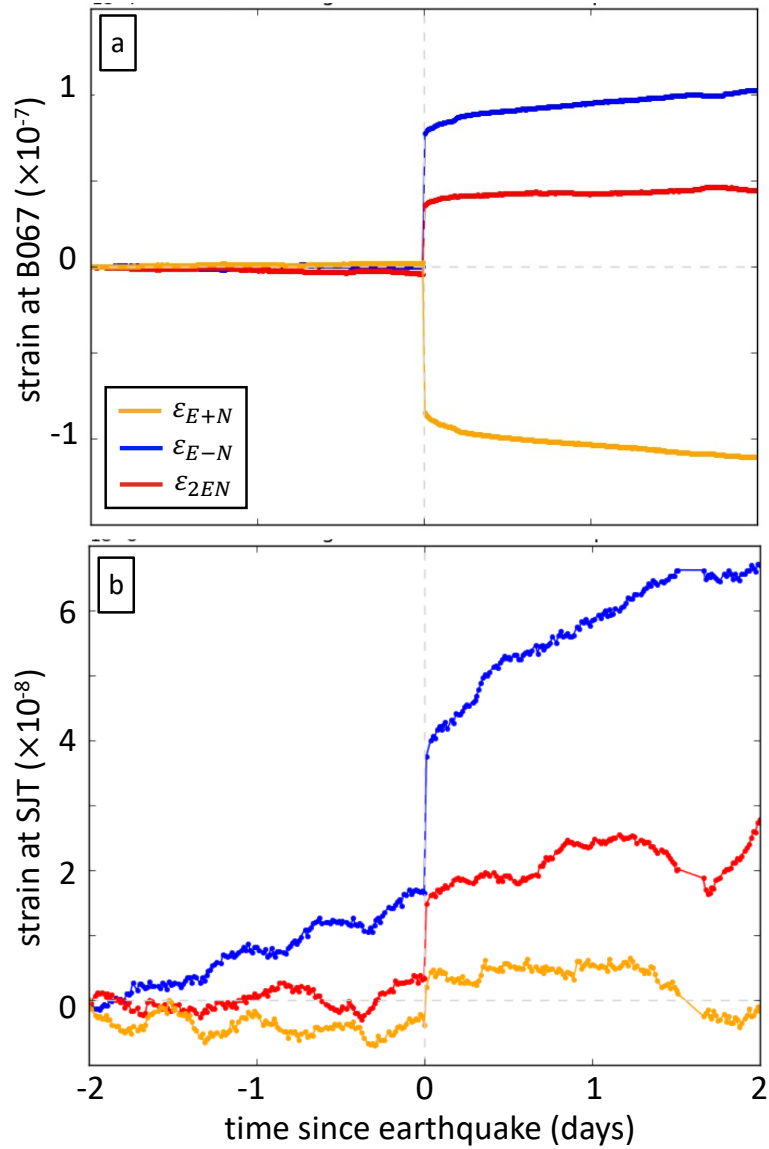


**Figure 2.** Illustrative records of co- and postseismic strain for (a) a  $M$  4.2 earthquake on 20-Nov-2015, recorded at B067 and located 5 km NE of the strainmeter at 6 km depth and (b) a  $M$  4.0 earthquake on 11-Feb-2001, recorded at SJT and located 5 km SE of the strainmeter at 6 km depth.

161 This selection does not bias our analysis toward small postseismic to coseismic moment  
 162 ratios because the noise in the strain data has a random walk character (Hawthorne &  
 163 Rubin, 2013; Langbein & Johnson, 1997). The uncertainty in the postseismic strain ac-  
 164 cumulation, which occurs over a few days, is larger than the uncertainty in the coseis-  
 165 mic strain accumulation. For the postseismic strain to be resolvable when the coseismic  
 166 strain is not, it would have to be about 10 times larger than the coseismic strain.

167 We do not analyze all records with well-resolved coseismic offsets, however. Some  
 168 are too complex to interpret because they occur within earthquake clusters or because  
 169 they trigger creep events. Creep events on the shallow San Andreas Fault are mostly hours-  
 170 to days-long intervals when part of the fault accelerates to rates of order mm to cm per  
 171 hour (Bilham, Suszek, & Pinkney, 2004; Gladwin, Gwyther, Hart, & Breckenbridge, 1994;  
 172 S. Schulz, Burford, & Mavko, 1983; S. S. Schulz, 1989; Thurber & Sessions, 1998). In  
 173 principle, creep events triggered by earthquakes can be classified as afterslip (e.g., Floyd  
 174 et al., 2016; Fukuda, Johnson, Larson, & Miyazaki, 2009; Langbein et al., 2006). We choose  
 175 to exclude creep events from our analysis for two reasons. First, it is unclear whether  
 176 the fault zone processes that create triggered creep events are the same as the processes  
 177 that usually create afterslip. The spontaneous occurrence of creep events suggest a par-  
 178 tially slip rate-weakening rheology that drives acceleration (e.g., Belardinelli, 1997; Wei,  
 179 Kaneko, Liu, & McGuire, 2013) while afterslip is often modeled with a slip rate-strengthening  
 180 rheology, so that increased slip rates are driven exclusively by the imposed coseismic stress  
 181 (Helmstetter & Shaw, 2009; Marone, Scholtz, & Bilham, 1991; Perfettini & Avouac, 2004).

182 Second, and more importantly, we exclude creep events because it is difficult to es-  
 183 timate their moments. As noted above, we can estimate the relative moment of after-  
 184 slip that is located close to the coseismic slip simply by computing the ratio of the post-  
 185 seismic to coseismic strain. But to estimate the relative moment of the triggered creep  
 186 events, we would need to account for the difference in Green’s functions between the co-  
 187 seismic rupture and the creep event slip. And we do not know the creep event locations  
 188 or the coseismic Green’s functions well enough to account for that difference. So we iden-  
 189 tify creep events by (1) looking at the nearby surface USGS creepmeter records and (2)  
 190 examining how the postseismic to coseismic strain ratio varies among the different com-  
 191 ponents of strain. The earthquakes excluded because of noise and nearby creep events  
 192 are listed in table S1.

## 193 **6 Estimates of Postseismic Strain**

194 After identifying earthquakes with well-resolved coseismic steps and excluding those  
 195 with visible creep events, we are left with 18 records, or 18 earthquake-station pairs, which  
 196 cover 14 independent earthquakes. We will estimate the coseismic and postseismic strain  
 197 of these earthquakes within a 1.5-day period. But first, we remove a linear trend that  
 198 may represent seasonal or hydrological variations. We estimate the trend from the strain  
 199 observations made in the two days before the earthquakes: by dividing the change in strain  
 200 between 2 days and 5 hours before the earthquake by that time interval (43 hours). We  
 201 extrapolate the estimated “long-term” strain rate through the co- and postseismic pe-  
 202 riod and subtract it from the strain time series. Note that the offset-over-time approach  
 203 to determining offsets and trends is appropriate for random walk noise, as appears to  
 204 characterize the strain data (Hawthorne & Rubin, 2013; Langbein & Johnson, 1997).

205 After removing the long-term trend, we estimate the coseismic and postseismic strain  
 206 changes for each of the three strain components. The coseismic strain change is defined  
 207 as the strain accumulated within the 40-minute interval centered on the earthquake time.  
 208 This 40-minute coseismic interval allows us to identify the entire coseismic strain step  
 209 from the 10- to 18-minute data. We interpolate between data points as necessary. The  
 210 postseismic strain change is defined as the strain that accumulates between 20 minutes  
 211 and 1.5 days after the earthquake. The 1.5-day interval is chosen as a compromise be-

212 tween signal and noise. It is long enough to allow significant strain to accumulate but  
 213 is short enough to avoid the large atmospheric and hydrological noise that can accumu-  
 214 late when longer time intervals are considered.

215 As noted earlier, we take the ratio of the postseismic to coseismic strains on each  
 216 component as an estimate of ratio of the postseismic to coseismic moments. To assess  
 217 how well resolved each postseismic moment ratio is, we examine how it would change  
 218 if noise were added. We randomly pick 3000 4-day-long intervals of the strain time se-  
 219 ries to use as 3000 realizations of the noise. We add each realization to the strain data  
 220 of interest, recompute and subtract a long-term trend, extract the coseismic and post-  
 221 seismic strain changes, and compute their ratio. With this approach, we obtain a prob-  
 222 ability distribution for the postseismic to coseismic moment ratios for each earthquake  
 223 and component. We identify and will examine the ratios from the earthquakes and com-  
 224 ponents that have reasonably low uncertainty ranges: those where 70% of the estimated  
 225 ratios fall within a range smaller than 2 (e.g., between 0 and 2, or between 0.5 and 2.5).  
 226 These ratios and their 70% confidence bounds are listed in table S2 and are plotted in  
 227 Figure 3a.

228 Most of the estimated postseismic to coseismic moment ratios cluster between 0  
 229 and 1. 64% of them are between 0.2 and 0.6. Note that two earthquakes, a  $M$  4.9 and  
 230 a  $M$  4.25, appear to have well-resolved but negative moment ratios. Such negative post-  
 231 seismic moment ratios would seem to imply that the fault is slipping backwards. How-  
 232 ever, the signal from the  $M$  4.9 may simply result from hydrological noise; there was sig-  
 233 nificant rainfall in January 1993, when the earthquake occurred (Figures S3 and S19).  
 234 The signal from the  $M$  4.25 is well resolved (Figure S10). But its postseismic to coseis-  
 235 mic moment ratios are different on the different components, suggesting that the post-  
 236 seismic strain may result from a triggered creep event, or from slip occurring in a dif-  
 237 ferent location than the coseismic slip. We choose to keep these two earthquakes in our  
 238 analysis because we had not excluded them before estimating the collection of moment  
 239 ratios.

240 Our goal here is not understand individual events, but to determine the typical af-  
 241 terslip moments of the available  $M$  4 to 5 earthquakes. The median of the estimated post-  
 242 seismic to coseismic moment ratios is 0.31. But it may be more appropriate to take the  
 243 median over earthquakes, to avoid overweighting a few events that have more than one  
 244 observation. So we group the estimated moment ratios by earthquake, take the median  
 245 for each group, and then take the median among the 12 unique earthquakes. The me-  
 246 dian earthquake-grouped moment ratio is 0.36.

247 To determine the uncertainty on the median moment ratio, we randomly pick sets  
 248 of values from the probability distributions for each earthquake and component, which  
 249 were obtained above by adding various realizations of the noise. We pick 4000 sets of ra-  
 250 tios and estimate their earthquake-grouped medians. Figure 3b shows a histogram of these  
 251 medians, which represents the probability distribution of the median postseismic to co-  
 252 seismic moment ratio. The distribution implies that the median postseismic ratio is be-  
 253 tween 0.28 and 0.48 with 70% probability and between 0.22 and 0.54 with 90% proba-  
 254 bility.

## 255 7 Discussion and Conclusion

256 The postseismic to coseismic moment ratios estimated here are plotted along with  
 257 the ratios inferred for smaller and larger earthquakes in Figures 4 and S20. The post-  
 258 seismic moments for smaller ( $M < 3.5$ ) earthquakes were obtained over the same time  
 259 interval considered here: from 20 minutes to 1.5 days after the earthquakes (Hawthorne,  
 260 Simons, & Ampuero, 2016). The postseismic observations of larger earthquakes were made  
 261 over a range of timescales, from days to years after the earthquakes. Postseismic moment



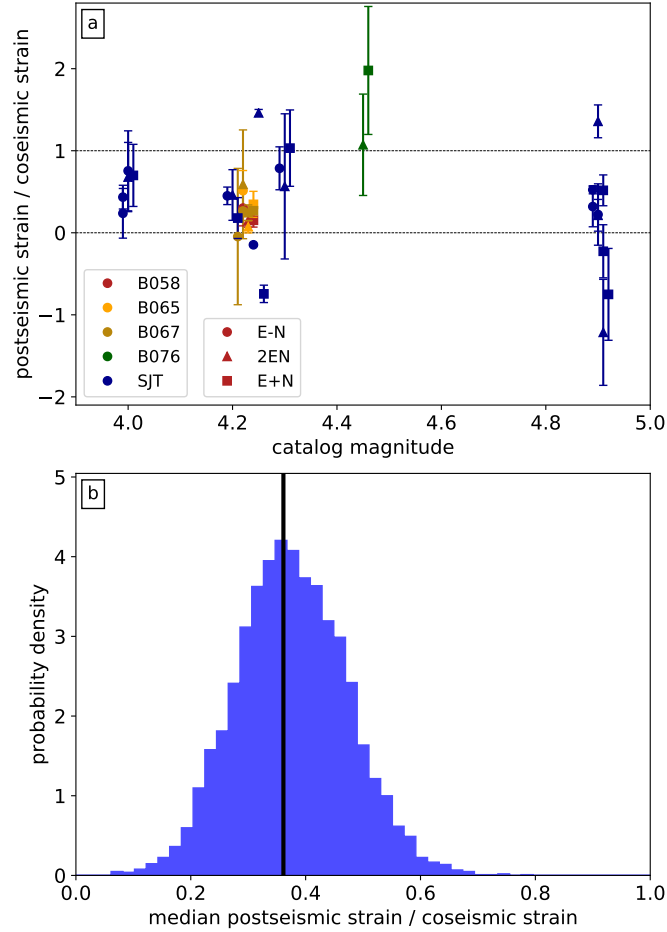


**Figure 3.** (a) Observed ratios of the postseismic strain changes, from 20 minutes to 1.5 days after the earthquakes, to the coseismic strain changes, from 20 minutes before to 20 minutes after the earthquakes. Each measurement comes from one component at one strainmeter, as indicated by color and symbol. Error bars indicate 70% uncertainty ranges. Note that we randomly shift the magnitudes by up to 0.015 to avoid plotting points on top of each other. (b) Vertical black line: median postseismic to coseismic strain ratio, obtained by taking the median over earthquakes. Probability distribution of the median postseismic to coseismic strain ratio, obtained by considering various realizations of the noise.

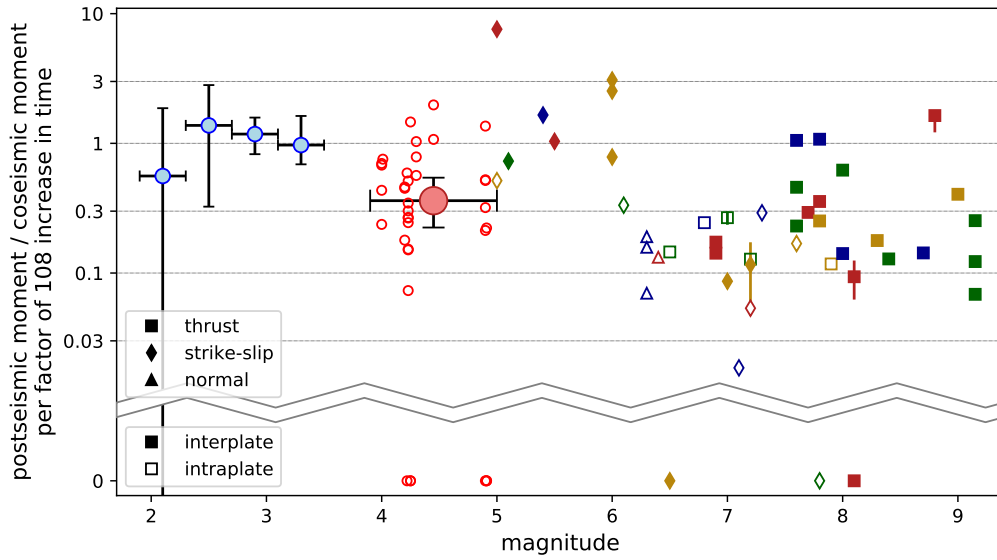


**Figure 4.** Time-normalized postseismic to coseismic moment ratios for earthquakes with a range of magnitudes. Note that the y-axis is on a log scale but that zero values are plotted below the break. The small red open circles are the individual measurements from this study, and the large red circle with error bars is the event-averaged median with 90% uncertainty ranges vertically and the range of magnitudes horizontally. The blue circles with error bars on the left are the moment ratios obtained by Hawthorne, Simons, and Ampuero (2016) for small earthquakes near San Juan Bautista, again with 90% uncertainty ranges vertically and the range of magnitudes horizontally. The points on the right come from a range of studies of intermediate and large-magnitude earthquakes, as listed in the text.

262 is often found to accumulate as the logarithm of time after the earthquake, so for a sim-  
 263 ple comparison in Figure 4, we normalize the larger earthquake observations to repre-  
 264 sent the moment accumulation expected for factor of 108 (=1.5 days / 15 minutes) in-  
 265 crease in time after the earthquake, assuming a logarithmic moment accumulation.

266 The postseismic to coseismic moment ratios we observe, with median 0.36, is slightly  
 267 larger than the moment typically seen after large ( $M > 6$ ) earthquakes. Most (though  
 268 not all) large earthquakes show postseismic moments smaller than 0.3 times the coseis-  
 269 mic moment (Amoruso & Crescentini, 2009; Barbot, Hamiel, & Fialko, 2008; Bürgmann  
 270 et al., 2001; Cetin et al., 2012; Cheloni et al., 2010; Chlieh et al., 2007; D’Agostino et  
 271 al., 2012; Diao, Wang, Wang, Xiong, & Walter, 2018; Dogan et al., 2014; Floyd et al.,  
 272 2016; Freed, 2007; Gonzalez-Ortega et al., 2014; Heki, Miyazaki, & Tsuji, 1997; Hobbs,  
 273 Kyriakopoulos, Newman, Protti, & Yao, 2017; Hsu et al., 2006; Jacobs, Sandwell, Fialko,  
 274 & Sichoix, 2002; Johanson & Bürgmann, 2010; Jónsson, 2008; Langbein et al., 2006; Lin  
 275 et al., 2013; Mahsas et al., 2008; Malservisi et al., 2015; Melbourne, Webb, Stock, & Reig-  
 276 ber, 2002; Miura, Suwa, Hasegawa, & Nishimura, 2004; Podgorski et al., 2007; Pritchard  
 277 & Simons, 2006; Rolandone et al., 2018; Ryder, Bürgmann, & Sun, 2010; Ryder et al.,  
 278 2007; Savage & Svarc, 1997; Segall et al., 2000; Shrivastava et al., 2016; Sreejith et al.,  
 279 2016; Subarya et al., 2006; Wen, Li, Xu, Ryder, & Bürgmann, 2012). Our  $M$  4 to 5 mo-  
 280 ment ratios are smaller than the reported moments for  $M$  5 to 6 earthquakes (Barbot  
 281 et al., 2009; Fattahi et al., 2015; Freed, 2007; Furuya & Satyabala, 2008; Langbein et al.,  
 282 2006; Murray-Moraleda & Simpson, 2009; Taira et al., 2014). But the high values for  $M$  5  
 283 to 6 earthquakes could result from observational bias; smaller postseismic moments may  
 284 not be reported because they would be harder to observe. More interestingly, then, we  
 285 note that our  $M$  4 to 5 moment ratios are also smaller than the roughly one to one ra-  
 286 tios observed for  $M < 3.5$  earthquakes Hawthorne, Simons, and Ampuero (2016).

287 There are several possible explanations for the observed variation in postseismic  
 288 moment with magnitude. First, the varying postseismic moments could reflect fault prop-  
 289 erties. Smaller earthquakes may be more likely to occur on creeping sections of faults,  
 290 perhaps on asperities surrounded by velocity-strengthening fault sections that are more  
 291 prone to large postseismic slip (e.g., Rolandone et al., 2018; Vaca, Vallée, Nocquet, Battaglia,  
 292 & Régnier, 2018). The postseismic moment estimates for  $M < 3.5$  earthquakes all come  
 293 from a single 20-km-wide fault segment near San Juan Bautista, CA, which could have  
 294 particular properties. But most of the earthquakes investigated here come from that same  
 295 fault segment, and half are obtained from measurements on the same strainmeter, SJT  
 296 (see Figures S1 to S10 for the time series).

297 It seems unlikely that other physical processes create some of the postseismic de-  
 298 formation we observe. Significant viscoelastic deformation is unlikely to accumulate on  
 299 the brief, 2-day timescale examined here (e.g., Bruhat, Barbot, & Avouac, 2011; John-  
 300 son, Bürgmann, & Freymueller, 2009; Pollitz, Banerjee, Burgmann, Hashimoto, & Choosakul,  
 301 2006). Poroelastic deformation can accumulate more quickly, but it typically has smaller  
 302 magnitude, just few percent of the coseismic deformation (Jónsson, Segall, Pedersen, &  
 303 Björnsson, 2003; Peltzer, Rosen, Rogez, & Hudnut, 1996, 1998) unless there is a nonlin-  
 304 ear near-surface response (e.g., Chia, Wang, Chiu, & Liu, 2001; Manga & Wang, 2007;  
 305 Quilty & Roeloffs, 1997; Wang, Wang, & Manga, 2004) or near-borehole deformation due  
 306 to shaking (Barbour, Agnew, & Wyatt, 2015), and Hawthorne, Simons, and Ampuero  
 307 (2016) identified no strong near-surface response to passing seismic waves or to creep events  
 308 in the San Juan Bautista region or at strainmeter SJT.

309 Assuming, then, that the postseismic deformation reflects afterslip, the magnitude-  
 310 dependent moment ratios could reflect the time intervals in which we observe that afterslip.  
 311 Postseismic moment is often observed to accumulate as log of the time  $t$  since  
 312 the earthquake, or at a rate of  $1/t$ . But at short times  $t$  after the earthquake, the mo-  
 313 ment rate may be slower than would be predicted by a  $1/t$  extrapolation, perhaps be-  
 314 cause the slipping region is growing outward from the coseismic rupture (Ariyoshi et al.,

2009; Dublanchet, Bernard, & Favreau, 2013a, 2013b; Lui & Lapusta, 2016; Perfettini & Ampuero, 2008) or because the fault takes time to accelerate in response to the coseismic stress increase (Marone et al., 1991; Montési, 2004; Perfettini & Avouac, 2004; Savage, 2007).

The coseismic rupture geometry can also influence the magnitude of postseismic slip. Small earthquakes tend to be more circular (e.g., Abercrombie, 1995; Gomberg, Wech, Creager, Obara, & Agnew, 2016; Scholz, 1982; Shaw, 2013), and thus may have a larger perimeter-to-area ratio and a larger region close to the coseismic rupture that can experience and respond to strong coseismic stress changes (Hawthorne, Simons, & Ampuero, 2016). However, the transition from circular to rectangular ruptures is typically inferred to occur when ruptures first start to span the seismogenic zone, at a magnitude around 6 or 7. We observe a change in postseismic moment at a magnitude of 4 to 5.

Alternatively, the magnitude-dependent postseismic moments could reflect a more fundamental property of earthquake dynamics. For instance, Chen and Lapusta (2009) identified large postseismic slip in rate and state friction models of earthquakes occurring on small asperities, on patches that were not much wider than the earthquake nucleation size. The large afterslip arose because portions of the potentially unstable asperities did not rupture in the earthquakes, and instead slipped via aseismic afterslip.

As observations of postseismic slip continue to accumulate, the ratio of postseismic to coseismic moment may become an important constraint on physical models of earthquake rupture. The postseismic moment ratios will complement observations of coseismic stress drops, which are usually found to be magnitude independent, suggesting that earthquakes are self-similar: that large earthquakes are scaled-up small earthquakes. In this study, we have made observations that appear to contradict self-similarity. The median postseismic moment estimated for the 12 well-resolved  $M$  4 to 5 earthquakes is 0.36 (0.22 to 0.54 with 90% probability). This afterslip moment of these intermediate-magnitude moments is intermediate relative to previous observations; it is slightly larger than is typical of  $M > 6$  earthquakes and smaller than observed for  $M < 3.5$  earthquakes.

### Acknowledgments

Strain and creep data for the San Juan Bautista (SJT) station are provided by the United States Geological Survey and are available at <http://earthquake.usgs.gov/monitoring/deformation/data/download/table.php>. The PBO strain data comes from stations operated by UNAVCO for EarthScope and supported by the National Science Foundation No. EAR-0350028 and EAR-0732947. It can be obtained via IRIS. The Northern California Seismic Network (NCSN) earthquake catalog is provided by the Northern California Earthquake Data Center and the Berkeley Seismological Laboratory (doi: 10.7932/NCEDC). The plotted fault traces come from the Quaternary fault and fold database, provided by the USGS and the California Geological Survey, and are available at <http://earthquake.usgs.gov/hazards/qfaults/>. The precipitation data used to interpret some records were provided by the National Oceanic and Atmospheric Administration (NOAA), and were accessed from <https://www.ncdc.noaa.gov/cdo-web/>.

### References

- Abercrombie, R. E. (1995). Earthquake source scaling relationships from -1 to 5 ML using seismograms recorded at 2.5-km depth. *J. Geophys. Res.*, *100*, 24015–24036. doi: 10.1029/95JB02397
- Amoruso, A., & Crescentini, L. (2009). Slow diffusive fault slip propagation following the 6 April 2009 L’Aquila earthquake, Italy. *Geophys. Res. Lett.*, *36*, L24306. doi: 10.1029/2009GL041503

- 364 Ariyoshi, K., Hori, T., Ampuero, J.-P., Kaneda, Y., Matsuzawa, T., Hino, R., &  
365 Hasegawa, A. (2009). Influence of interaction between small asperities on  
366 various types of slow earthquakes in a 3-D simulation for a subduction plate  
367 boundary. *Gondwana Res.*, *16*(3-4), 534–544. doi: 10.1016/j.gr.2009.03.006
- 368 Barbot, S., Fialko, Y., & Bock, Y. (2009). Postseismic deformation due to the Mw  
369 6.0 2004 Parkfield earthquake: Stress-driven creep on a fault with spatially  
370 variable rate-and-state friction parameters. *J. Geophys. Res.*, *114*, B07405.  
371 doi: 10.1029/2008JB005748
- 372 Barbot, S., Hamiel, Y., & Fialko, Y. (2008). Space geodetic investigation of the co-  
373 seismic and postseismic deformation due to the 2003 Mw 7.2 Altai earthquake:  
374 Implications for the local lithospheric rheology. *J. Geophys. Res.*, *113*, B03403.  
375 doi: 10.1029/2007JB005063
- 376 Barbour, A. J., Agnew, D. C., & Wyatt, F. K. (2015). Coseismic strains on Plate  
377 Boundary Observatory borehole strainmeters in southern California. *Bull. Seis.*  
378 *Soc. Amer.*, *105*(1), 431–444. doi: 10.1785/0120140199
- 379 Belardinelli, M. E. (1997). Increase of creep interevent intervals: a conceptual model.  
380 *Tectonophysics*, *277*(1-3), 99–107. doi: 10.1016/S0040-1951(97)00080-2
- 381 Bell, J. W., Amelung, F., & Henry, C. D. (2012). InSAR analysis of the 2008  
382 Reno-Mogul earthquake swarm: Evidence for westward migration of Walker  
383 Lane style dextral faulting. *Geophys. Res. Lett.*, *39*(18), L18306. doi:  
384 10.1029/2012GL052795
- 385 Bilham, R., Suszek, N., & Pinkney, S. (2004). California Creepmeters. *Seis. Res.*  
386 *Lett.*, *75*(4), 481–492. doi: 10.1785/gssrl.75.4.481
- 387 Bruhat, L., Barbot, S., & Avouac, J.-P. (2011). Evidence for postseismic deformation  
388 of the lower crust following the 2004 Mw6.0 Parkfield earthquake. *J. Geo-*  
389 *phys. Res.*, *116*(B8), B08401. doi: 10.1029/2010JB008073
- 390 Bürgmann, R., Kogan, M. G., Levin, V. E., Scholz, C. H., King, R. W., & Steblov,  
391 G. M. (2001). Rapid aseismic moment release following the 5 December, 1997  
392 Kronotsky, Kamchatka, Earthquake. *Geophys. Res. Lett.*, *28*(7), 1331–1334.  
393 doi: 10.1029/2000GL012350
- 394 Cartwright, D. E., & Edden, A. C. (1973). Corrected tables of tidal harmonics. *Geo-*  
395 *phys. J. Intern.*, *33*(3), 253–264. doi: 10.1111/j.1365-246X.1973.tb03420.x
- 396 Cetin, E., Meghraoui, M., Cakir, Z., Akoglu, A. M., Mimouni, O., & Chebbah, M.  
397 (2012). Seven years of postseismic deformation following the 2003 Mw 6.8  
398 Zemmouri earthquake (Algeria) from InSAR time series. *Geophys. Res. Lett.*,  
399 *39*(10), L10307. doi: 10.1029/2012GL051344
- 400 Cheloni, D., D’Agostino, N., D’Anastasio, E., Avallone, A., Mantenuto, S., Giuliani,  
401 R., . . . Fastellini, G. (2010). Coseismic and initial post-seismic slip of the  
402 2009 Mw 6.3 L’Aquila earthquake, Italy, from GPS measurements. *Geophys. J.*  
403 *Intern.*, *181*(3), 1539–1546. doi: 10.1111/j.1365-246X.2010.04584.x
- 404 Chen, T., & Lapusta, N. (2009). Scaling of small repeating earthquakes explained by  
405 interaction of seismic and aseismic slip in a rate and state fault model. *J. Geo-*  
406 *phys. Res.*, *114*, B01311. doi: 10.1029/2008JB005749
- 407 Chia, Y., Wang, Y.-S., Chiu, J. J., & Liu, C.-W. (2001). Changes of groundwater  
408 level due to the 1999 Chi-Chi earthquake in the Choshui River alluvial fan in  
409 Taiwan. *Bull. Seis. Soc. Amer.*, *91*(5), 1062–1068. doi: 10.1785/0120000726
- 410 Chlieh, M., Avouac, J.-P., Hjorleifsdottir, V., Song, T.-R. A., Ji, C., Sieh, K., . . .  
411 Galetzka, J. (2007). Coseismic slip and afterslip of the great Mw 9.15 Suma-  
412 tra–Andaman earthquake of 2004. *Bull. Seis. Soc. Amer.*, *97*(1A), S152–S173.  
413 doi: 10.1785/0120050631
- 414 D’Agostino, N., Cheloni, D., Fornaro, G., Giuliani, R., & Reale, D. (2012). Space-  
415 time distribution of afterslip following the 2009 L’Aquila earthquake. *J. Geo-*  
416 *phys. Res.*, *117*(B2), B02402. doi: 10.1029/2011JB008523
- 417 Diao, F., Wang, R., Wang, Y., Xiong, X., & Walter, T. R. (2018). Fault behavior  
418 and lower crustal rheology inferred from the first seven years of postseismic

- 419 GPS data after the 2008 Wenchuan earthquake. *Earth Planet. Sci. Lett.*, *495*,  
 420 202–212. doi: 10.1016/j.epsl.2018.05.020
- 421 Dogan, U., Demir, D. Ö., Çakir, Z., Ergintav, S., Ozener, H., Akoğlu, A. M., ...  
 422 Reilinger, R. (2014). Postseismic deformation following the Mw 7.2, 23 Oc-  
 423 tober 2011 Van earthquake (Turkey): Evidence for aseismic fault reactivation.  
 424 *Geophys. Res. Lett.*, *41*(7), 2334–2341. doi: 10.1002/2014GL059291
- 425 Donnellan, A., & Lyzenga, G. A. (1998). GPS observations of fault afterslip and up-  
 426 per crustal deformation following the Northridge earthquake. *J. Geophys. Res.*,  
 427 *103*(B9), 21285–21297. doi: 10.1029/98JB01487
- 428 Dublanchet, P., Bernard, P., & Favreau, P. (2013a). Creep modulation of Omori law  
 429 generated by a Coulomb stress perturbation in a 3-D rate-and-state asperity  
 430 model. *J. Geophys. Res.*, *118*(9), 4774–4793. doi: 10.1002/jgrb.50311
- 431 Dublanchet, P., Bernard, P., & Favreau, P. (2013b). Interactions and triggering in a  
 432 3-D rate-and-state asperity model. *J. Geophys. Res.*, *118*(5), 2225–2245. doi:  
 433 10.1002/jgrb.50187
- 434 Fattahi, H., Amelung, F., Chaussard, E., & Wdowinski, S. (2015). Coseismic  
 435 and postseismic deformation due to the 2007 M5.5 Ghazaband fault earth-  
 436 quake, Balochistan, Pakistan. *Geophys. Res. Lett.*, *42*(9), 3305–3312. doi:  
 437 10.1002/2015GL063686
- 438 Floyd, M. A., Walters, R. J., Elliott, J. R., Funning, G. J., Svarc, J. L., Murray,  
 439 J. R., ... Wright, T. J. (2016). Spatial variations in fault friction related to  
 440 lithology from rupture and afterslip of the 2014 South Napa, California, earth-  
 441 quake. *Geophys. Res. Lett.*, *43*(13), 6808–6816. doi: 10.1002/2016GL069428
- 442 Freed, A. M. (2007). Afterslip (and only afterslip) following the 2004 Parkfield,  
 443 California, earthquake. *Geophys. Res. Lett.*, *34*(6), L06312. doi: 10.1029/  
 444 2006GL029155
- 445 Fukuda, J., Johnson, K. M., Larson, K. M., & Miyazaki, S. (2009). Fault friction pa-  
 446 rameters inferred from the early stages of afterslip following the 2003 Tokachi-  
 447 oki earthquake. *J. Geophys. Res.*, *114*, B04412. doi: 10.1029/2008JB006166
- 448 Furuya, M., & Satyabala, S. P. (2008). Slow earthquake in Afghanistan detected by  
 449 InSAR. *Geophys. Res. Lett.*, *35*(6), L06309. doi: 10.1029/2007GL033049
- 450 Gahalaut, V. K., Jade, S., Catherine, J. K., Gireesh, R., Ananda, M. B., Kumar,  
 451 P. D., ... Kumar, S. (2008). GPS measurements of postseismic deformation  
 452 in the Andaman-Nicobar region following the giant 2004 Sumatra-Andaman  
 453 earthquake. *J. Geophys. Res.*, *113*(B8), B08401. doi: 10.1029/2007JB005511
- 454 Gladwin, M. T., Gwyther, R. L., Hart, R., Francis, M., & Johnston, M. J. S. (1987).  
 455 Borehole tensor strain measurements in California. *J. Geophys. Res.*, *92*(B8),  
 456 7981–7988. doi: 10.1029/JB092iB08p07981
- 457 Gladwin, M. T., Gwyther, R. L., Hart, R. H. G., & Breckenbridge, K. S. (1994).  
 458 Measurements of the strain field associated with episodic creep events on the  
 459 San Andreas fault at San Juan Bautista, California. *J. Geophys. Res.*, *99*,  
 460 4559–4565. doi: 10.1029/93JB02877
- 461 Gomberg, J., Wech, A., Creager, K., Obara, K., & Agnew, D. (2016). Reconsider-  
 462 ing earthquake scaling. *Geophys. Res. Lett.*, *43*(12), 6243–6251. doi: 10.1002/  
 463 2016GL069967
- 464 Gonzalez-Ortega, A., Fialko, Y., Sandwell, D., Alejandro Nava-Pichardo, F.,  
 465 Fletcher, J., Gonzalez-Garcia, J., ... Funning, G. (2014). El Mayor-Cucapah  
 466 (Mw 7.2) earthquake: Early near-field postseismic deformation from In-  
 467 SAR and GPS observations. *J. Geophys. Res.*, *119*(2), 1482–1497. doi:  
 468 10.1002/2013JB010193
- 469 Hart, R. H. G., Gladwin, M. T., Gwyther, R. L., Agnew, D. C., & Wyatt, F. K.  
 470 (1996). Tidal calibration of borehole strain meters: Removing the effects of  
 471 small-scale inhomogeneity. *J. Geophys. Res.*, *101*(B11), 25553–25571. doi:  
 472 10.1029/96JB02273
- 473 Hawthorne, J. C., Bostock, M. G., Royer, A. A., & Thomas, A. M. (2016).

- 474 Variations in slow slip moment rate associated with rapid tremor rever-  
 475 sals in Cascadia. *Geochem., Geophys., Geosyst.*, *17*(12), 4899–4919. doi:  
 476 10.1002/2016GC006489
- 477 Hawthorne, J. C., & Rubin, A. M. (2013). Short-time scale correlation between slow  
 478 slip and tremor in Cascadia. *J. Geophys. Res.*, *118*(3), 1316–1329. doi: 10  
 479 .1002/jgrb.50103
- 480 Hawthorne, J. C., Simons, M., & Ampuero, J.-P. (2016). Estimates of aseismic slip  
 481 associated with small earthquakes near San Juan Bautista, CA. *J. Geophys.*  
 482 *Res.*, *121*(11), 8254–8275. doi: 10.1002/2016JB013120
- 483 Heki, K., Miyazaki, S., & Tsuji, H. (1997). Silent fault slip following an interplate  
 484 thrust earthquake at the Japan Trench. *Nature*, *386*(6625), 595–598. doi: 10  
 485 .1038/386595a0
- 486 Helmstetter, A., & Shaw, B. E. (2009). Afterslip and aftershocks in the rate-and-  
 487 state friction law. *J. Geophys. Res.*, *114*, B01308. doi: 10.1029/2007JB005077
- 488 Hobbs, T. E., Kyriakopoulos, C., Newman, A. V., Protti, M., & Yao, D. (2017).  
 489 Large and primarily updip afterslip following the 2012 Mw 7.6 Nicoya,  
 490 Costa Rica, earthquake. *J. Geophys. Res.*, *122*(7), 5712–5728. doi:  
 491 10.1002/2017JB014035
- 492 Hodgkinson, K., Langbein, J., Henderson, B., Mencin, D., & Borsa, A. (2013). Tidal  
 493 calibration of Plate Boundary Observatory borehole strainmeters. *J. Geophys.*  
 494 *Res.*, *118*(1), 447–458. doi: 10.1029/2012JB009651
- 495 Hsu, Y.-J., Simons, M., Avouac, J.-P., Galetzka, J., Sieh, K., Chlieh, M., . . . Bock,  
 496 Y. (2006). Frictional afterslip following the 2005 Nias-Simeulue earthquake,  
 497 Sumatra. *Science*, *312*(5782), 1921–1926. doi: 10.1126/science.1126960
- 498 Irwin, W. P., & Barnes, I. (1975). Effect of geologic structure and metamorphic flu-  
 499 ids on seismic behavior of the San Andreas fault system in central and north-  
 500 ern California. *Geology*, *3*(12), 713–716. doi: 10.1130/0091-7613(1975)3<713:  
 501 EOGSAM>2.0.CO;2
- 502 Jacobs, A., Sandwell, D., Fialko, Y., & Sichoix, L. (2002). The 1999 (Mw 7.1)  
 503 Hector Mine, California, earthquake: near-field postseismic deformation  
 504 from ERS interferometry. *Bull. Seis. Soc. Amer.*, *92*(4), 1433–1442. doi:  
 505 10.1785/0120000908
- 506 Johanson, I. A., & Bürgmann, R. (2010). Coseismic and postseismic slip from  
 507 the 2003 San Simeon earthquake and their effects on backthrust slip and  
 508 the 2004 Parkfield earthquake. *J. Geophys. Res.*, *115*(B7), B07411. doi:  
 509 10.1029/2009JB006599
- 510 Johnson, K. M., Bürgmann, R., & Freymueller, J. T. (2009). Coupled afterslip and  
 511 viscoelastic flow following the 2002 Denali Fault, Alaska earthquake. *Geophys.*  
 512 *J. Intern.*, *176*(3), 670–682. doi: 10.1111/j.1365-246X.2008.04029.x
- 513 Jónsson, S. (2008). Importance of post-seismic viscous relaxation in southern Ice-  
 514 land. *Nat. Geosci.*, *1*(2), 136–139. doi: 10.1038/ngeo105
- 515 Jónsson, S., Segall, P., Pedersen, R., & Björnsson, G. (2003). Post-earthquake  
 516 ground movements correlated to pore-pressure transients. *Nature*, *424*(6945),  
 517 179–183. doi: 10.1038/nature01776
- 518 Langbein, J. (2010). Computer algorithm for analyzing and processing borehole  
 519 strainmeter data. *Computers & Geosciences*, *36*(5), 611–619. doi: 10.1016/j  
 520 .cageo.2009.08.011
- 521 Langbein, J., & Johnson, H. (1997). Correlated errors in geodetic time series: Impli-  
 522 cations for time-dependent deformation. *J. Geophys. Res.*, *102*(B1), 591–603.  
 523 doi: 199710.1029/96JB02945
- 524 Langbein, J., Murray, J. R., & Snyder, H. A. (2006). Coseismic and initial post-  
 525 seismic deformation from the 2004 Parkfield, California, earthquake, observed  
 526 by global positioning system, electronic distance meter, creepmeters, and  
 527 borehole strainmeters. *Bull. Seis. Soc. Amer.*, *96*(4B), S304–S320. doi:  
 528 10.1785/0120050823

- 529 Lin, Y.-n. N., Sladen, A., Ortega-Culaciati, F., Simons, M., Avouac, J.-P., Field-  
530 ing, E. J., . . . Socquet, A. (2013). Coseismic and postseismic slip associated  
531 with the 2010 Maule Earthquake, Chile: Characterizing the Arauco Peninsula  
532 barrier effect. *J. Geophys. Res.*, *118*(6), 3142–3159. doi: 10.1002/jgrb.50207
- 533 Lui, S. K. Y., & Lapusta, N. (2016). Repeating microearthquake sequences interact  
534 predominantly through postseismic slip. *Nat. Comm.*, *7*, ncomms13020. doi:  
535 10.1038/ncomms13020
- 536 Mahsas, A., Lammali, K., Yelles, K., Calais, E., Freed, A. M., & Briole, P. (2008).  
537 Shallow afterslip following the 2003 May 21, Mw= 6.9 Boumerdes earth-  
538 quake, Algeria. *Geophys. J. Intern.*, *172*(1), 155–166. doi: 10.1111/  
539 j.1365-246X.2007.03594.x
- 540 Malservisi, R., Schwartz, S. Y., Voss, N., Protti, M., Gonzalez, V., Dixon, T. H., . . .  
541 Voyenko, D. (2015). Multiscale postseismic behavior on a megathrust: The  
542 2012 Nicoya earthquake, Costa Rica. *Geochem., Geophys., Geosyst.*, *16*(6),  
543 1848–1864. doi: 10.1002/2015GC005794
- 544 Manga, M., & Wang, C.-Y. (2007). Earthquake hydrology. In Hiroo Kanamori &  
545 G. Schubert (Eds.), *Treatise on Geophysics* (Vol. 4: Earthquake Seismology,  
546 p. 6054). Amsterdam: Elsevier.
- 547 Marone, C. J., Scholtz, C. H., & Bilham, R. (1991). On the mechanics of earthquake  
548 afterslip. *J. Geophys. Res.*, *96*(B5), 8441–8452. doi: 10.1029/91JB00275
- 549 Melbourne, T. I., Webb, F. H., Stock, J. M., & Reigber, C. (2002). Rapid post-  
550 seismic transients in subduction zones from continuous GPS. *J. Geophys. Res.*,  
551 *107*(B10), 2241. doi: 10.1029/2001JB000555
- 552 Miura, S., Suwa, Y., Hasegawa, A., & Nishimura, T. (2004). The 2003 M8.0  
553 Tokachi-Oki earthquake – How much has the great event paid back slip debts?  
554 *Geophys. Res. Lett.*, *31*(5), L05613. doi: 10.1029/2003GL019021
- 555 Montési, L. G. J. (2004). Controls of shear zone rheology and tectonic load-  
556 ing on postseismic creep. *J. Geophys. Res.*, *109*(B10), B10404. doi:  
557 10.1029/2003JB002925
- 558 Murray-Moraleda, J. R., & Simpson, R. W. (2009). Geodetically inferred coseismic  
559 and postseismic slip due to the M 5.4 31 October 2007 Alum Rock earthquake.  
560 *Bull. Seis. Soc. Amer.*, *99*(5), 2784–2800. doi: 10.1785/0120090017
- 561 Paul, J., Lowry, A. R., Bilham, R., Sen, S., & Smalley, R. (2007). Postseis-  
562 mic deformation of the Andaman Islands following the 26 December, 2004  
563 Great Sumatra-Andaman earthquake. *Geophys. Res. Lett.*, *34*, L19309. doi:  
564 10.1029/2007GL031024
- 565 Peltzer, G., Rosen, P., Rogez, F., & Hudnut, K. (1996). Postseismic rebound in fault  
566 step-overs caused by pore fluid flow. *Science*, *273*(5279), 1202–1204. doi: 10  
567 .1126/science.273.5279.1202
- 568 Peltzer, G., Rosen, P., Rogez, F., & Hudnut, K. (1998). Poroelastic rebound along  
569 the Landers 1992 earthquake surface rupture. *J. Geophys. Res.*, *103*(B12),  
570 30131–30145. doi: 10.1029/98JB02302
- 571 Perfettini, H., & Ampuero, J. P. (2008). Dynamics of a velocity strengthening fault  
572 region: Implications for slow earthquakes and postseismic slip. *J. Geophys.*  
573 *Res.*, *113*, B09411. doi: 10.1029/2007JB005398
- 574 Perfettini, H., & Avouac, J. P. (2004). Postseismic relaxation driven by brittle creep:  
575 A possible mechanism to reconcile geodetic measurements and the decay rate  
576 of aftershocks, application to the Chi-Chi earthquake, Taiwan. *J. Geophys.*  
577 *Res.*, *109*, B02304. doi: 10.1029/2003JB002488
- 578 Podgorski, J., Hearn, E. H., McClusky, S., Reilinger, R., Taymaz, T., Tan, O.,  
579 . . . Nadariya, M. (2007). Postseismic deformation following the 1991  
580 Racha, Georgia, earthquake. *Geophys. Res. Lett.*, *34*(4), L04310. doi:  
581 10.1029/2006GL028477
- 582 Pollitz, F. F., Banerjee, P., Burgmann, R., Hashimoto, M., & Choosakul, N. (2006).  
583 Stress changes along the Sunda trench following the 26 December 2004



- 584 Sumatra-Andaman and 28 March 2005 Nias earthquakes. *Geophys. Res.*  
 585 *Lett.*, *33*(6), L06309. doi: 10.1029/2005GL024558
- 586 Pritchard, M. E., & Simons, M. (2006). An aseismic slip pulse in northern Chile and  
 587 along-strike variations in seismogenic behavior. *J. Geophys. Res.*, *111*, B08405.  
 588 doi: 10.1029/2006JB004258
- 589 Quilty, E. G., & Roeloffs, E. A. (1997). Water-level changes in response to the 20  
 590 December 1994 earthquake near Parkfield, California. *Bull. Seis. Soc. Amer.*,  
 591 *87*(2), 310–317.
- 592 Roeloffs, E. (2010). Tidal calibration of Plate Boundary Observatory borehole  
 593 strainmeters: Roles of vertical and shear coupling. *J. Geophys. Res.*, *115*,  
 594 B06405. doi: 10.1029/2009JB006407
- 595 Rolandone, F., Nocquet, J.-M., Mothes, P. A., Jarrin, P., Vallée, M., Cubas, N., ...  
 596 Font, Y. (2018). Areas prone to slow slip events impede earthquake rupture  
 597 propagation and promote afterslip. *Science Advances*, *4*(1), eaao6596. doi:  
 598 10.1126/sciadv.aao6596
- 599 Ryder, I., Bürgmann, R., & Sun, J. (2010). Tandem afterslip on connected fault  
 600 planes following the 2008 Nima-Gaize (Tibet) earthquake. *J. Geophys. Res.*,  
 601 *115*(B3), B03404. doi: 10.1029/2009JB006423
- 602 Ryder, I., Parsons, B., Wright, T. J., & Funning, G. J. (2007). Post-seismic  
 603 motion following the 1997 Manyi (Tibet) earthquake: InSAR observa-  
 604 tions and modelling. *Geophys. J. Intern.*, *169*(3), 1009–1027. doi:  
 605 10.1111/j.1365-246X.2006.03312.x
- 606 Savage, J. C. (2007). Postseismic relaxation associated with transient creep rheology.  
 607 *J. Geophys. Res.*, *112*, B05412. doi: 10.1029/2006JB004688
- 608 Savage, J. C., & Svarc, J. L. (1997). Postseismic deformation associated with the  
 609 1992 Mw 7.3 Landers earthquake, southern California. *J. Geophys. Res.*,  
 610 *102*(B4), 7565–7577. doi: 10.1029/97JB00210
- 611 Scholz, C. H. (1982). Scaling laws for large earthquakes: Consequences for physical  
 612 models. *Bull. Seis. Soc. Amer.*, *72*(1), 1–14.
- 613 Schulz, S., Burford, R. O., & Mavko, B. (1983). Influence of seismicity and rainfall  
 614 on episodic creep on the San Andreas Fault System in central California. *J.*  
 615 *Geophys. Res.*, *88*(B9), 7475–7484. doi: 10.1029/JB088iB09p07475
- 616 Schulz, S. S. (1989). *Catalog of creepmeter measurements in California from 1966*  
 617 *through 1988* (Tech. Rep. No. 89-650). USGS. (Version 1.1)
- 618 Segall, P., Bürgmann, R., & Matthews, M. (2000). Time-dependent triggered afterslip  
 619 following the 1989 Loma Prieta earthquake. *J. Geophys. Res.*, *105*(B3),  
 620 5615–5634. doi: 10.1029/1999JB900352
- 621 Shaw, B. E. (2013). Earthquake surface slip-length data is fit by constant stress  
 622 drop and is useful for seismic hazard analysis. *Bull. Seis. Soc. Amer.*, *103*(2A),  
 623 876–893. doi: 10.1785/0120110258
- 624 Shrivastava, M. N., González, G., Moreno, M., Chlieh, M., Salazar, P., Reddy, C. D.,  
 625 ... de la Llera, J. C. (2016). Coseismic slip and afterslip of the 2015 Mw 8.3  
 626 Illapel (Chile) earthquake determined from continuous GPS data. *Geophys.*  
 627 *Res. Lett.*, *43*(20), 2016GL070684. doi: 10.1002/2016GL070684
- 628 Sreejith, K. M., Sunil, P. S., Agrawal, R., Saji, A. P., Ramesh, D. S., & Rajawat,  
 629 A. S. (2016). Coseismic and early postseismic deformation due to the 25 April  
 630 2015, Mw 7.8 Gorkha, Nepal, earthquake from InSAR and GPS measurements.  
 631 *Geophys. Res. Lett.*, *43*(7), 2016GL067907. doi: 10.1002/2016GL067907
- 632 Subarya, C., Chlieh, M., Prawirodirdjo, L., Avouac, J. P., Bock, Y., Sieh, K.,  
 633 ... McCaffrey, R. (2006). Plate-boundary deformation associated with  
 634 the great Sumatra-Andaman earthquake. *Nature*, *440*(7080), 46–51. doi:  
 635 10.1038/nature04522
- 636 Taira, T., Bürgmann, R., Nadeau, R. M., & Dreger, D. S. (2014). Variability of fault  
 637 slip behavior along the San Andreas Fault in the San Juan Bautista Region. *J.*  
 638 *Geophys. Res.*, *119*(12), 8827–8844. doi: 10.1002/2014JB011427

- 639 Thurber, C., & Sessions, R. (1998). Assessment of creep events as potential earth-  
640 quake precursors: application to the creeping section of the San Andreas Fault,  
641 California. *Pure Appl. Geophys.*, *152*, 685–705. doi: 10.1007/s000240050172
- 642 Vaca, S., Vallée, M., Nocquet, J.-M., Battaglia, J., & Régnier, M. (2018). Recurrent  
643 slow slip events as a barrier to the northward rupture propagation of the 2016  
644 Pedernales earthquake (Central Ecuador). *Tectonophysics*, *724-725*, 80–92.  
645 doi: 10.1016/j.tecto.2017.12.012
- 646 Waldhauser, F., & Schaff, D. P. (2008). Large-scale relocation of two decades of  
647 Northern California seismicity using cross-correlation and double-difference  
648 methods. *J. Geophys. Res.*, *113*(B8), B08311. doi: 10.1029/2007JB005479
- 649 Wang, C.-y., Wang, C.-H., & Manga, M. (2004). Coseismic release of water from  
650 mountains: Evidence from the 1999 (Mw = 7.5) Chi-Chi, Taiwan, earthquake.  
651 *Geology*, *32*(9), 769–772. doi: 10.1130/G20753.1
- 652 Wei, M., Kaneko, Y., Liu, Y., & McGuire, J. J. (2013). Episodic fault creep events  
653 in California controlled by shallow frictional heterogeneity. *Nat. Geosci.*, *6*(7),  
654 566–570. doi: 10.1038/ngeo1835
- 655 Wen, Y., Li, Z., Xu, C., Ryder, I., & Bürgmann, R. (2012). Postseismic motion after  
656 the 2001 Mw 7.8 Kokoxili earthquake in Tibet observed by InSAR time series.  
657 *J. Geophys. Res.*, *117*(B8), B08405. doi: 10.1029/2011JB009043